catalysts

MDPI

Article

Activated Carbon Assisted Fenton-like Treatment of Wastewater Containing Acid Red G

Xuanye Yan [1], Hang Li [1], Jiangtao Feng [1,*], Bo Hou [2,*], Wei Yan [1,3] and Min Zhou [4]

[1] Department of Environmental Engineering, Xi'an Key Laboratory of Solid Waste Recycling and Resource Recovery, School of Energy and Power Engineering, Xi'an Jiaotong University, Xi'an 710049, China
[2] School of Physics and Astronomy, Cardiff University, Cardiff CF24 3AA, UK
[3] Jiangsu Engineering Laboratory of New Materials for Sewage Treatment and Recycling, Soochow University, Suzhou 215123, China
[4] Peng'an Ecological Environment Monitoring Station, Nanchong 637800, China
* Correspondence: fjtes@xjtu.edu.cn (J.F.); HouB6@cardiff.ac.uk (B.H.)

Abstract: The Fenton reaction as an effective advanced oxidation technology has been widely used in wastewater treatment for its stable effluent quality, simple operation, mild condition, and higher organic degradation with non-selectivity. However, the traditional Fenton reaction is limited by the sluggish regeneration of Fe^{2+}, resulting in a slower reaction rate, and it is necessary to further increase the dosage of Fe^{2+}, which will increase the production of iron sludge. Activated carbon (AC) has a strong adsorption property, and it cannot be ignored that it also can reduce Fe^{3+}. In this study, the degradation of acid red G (ARG) by adding AC to the Fe^{3+}/H_2O_2 system, the role of the reducing ability, and the reason why AC can reduce Fe^{3+} were studied. By adding three kinds of ACs, including coconut shell-activated carbon (CSPAC), wood-activated carbon (WPAC), and coal-activated carbon (CPAC), the ability of ACs to assist the Fe^{3+}/H_2O_2 Fenton-like system to degrade ARG was clarified. Through the final treatment effect and the ability to reduce Fe^{3+}, the type of AC with the best promotion effect was CSPAC. The different influence factors of particle size, the concentration of CSPAC, concentration of H_2O_2, concentration of Fe^{3+}, and pH value were further observed. The best reaction conditions were determined as CSPAC powder with a particle size of 75 μm and dosage of 0.6 g/L, initial H_2O_2 concentration of 0.4 mmol/L, Fe^{3+} concentration of 0.1 mmol/L, and pH = 3. By reducing the adsorption effect of CSPAC, it was further observed that CSPAC could accelerate the early reaction rate of the degradation process of ARG by the Fe^{3+}/H_2O_2 system. FT-IR and XPS confirmed that the C-O-H group on the surface of CSPAC could reduce Fe^{3+} to Fe^{2+}. This study can improve the understanding and role of AC in the Fenton reaction, and further promote the application of the Fenton reaction in sewage treatment.

Keywords: Fenton reaction; activated carbon; reduction of Fe^{3+}; adsorption; acid red G (ARG)

Citation: Yan, X.; Li, H.; Feng, J.; Hou, B.; Yan, W.; Zhou, M. Activated Carbon Assisted Fenton-like Treatment of Wastewater Containing Acid Red G. *Catalysts* **2022**, *12*, 1358. https://doi.org/10.3390/catal12111358

Academic Editor: Enric Brillas

Received: 27 September 2022
Accepted: 25 October 2022
Published: 3 November 2022

1. Introduction

The Fenton reaction as one of the effective advanced oxidation technologies (AOPs) has been widely used in wastewater treatment for its stable effluent quality, simple operation, higher organic loading, and mild condition [1–3]. For instance, the Fenton process can dispose of wastewater with a large chemical oxygen demand (COD) ranging from 100,000 to 150,000 mg/L [4,5]. Meanwhile, the Fenton reaction can degrade not only conventional organic pollutants but also bioaccumulated and refractory pollutants, such as high-concentration nitrogenous dye [6–10], estrogens, and antibiotics. Fenton process can also be applied to soil remediation [11–13], biomedicine [14], treating deep bacteria-infected diseases [15], and water treatment due to its lower side effects and lack of equipment restrictions.

However, the Fenton reaction mainly relies on the core reaction between Fe^{2+} and H_2O_2 at low pH conditions (pH of 2–4) to generate hydroxyl radicals (•OH) for efficient

degradation of organic matter in water with non-selectivity [16,17]. In the reaction process, Fe^{2+} is oxidized to Fe^{3+}. Although the generated Fe^{3+} can be reduced by H_2O_2 to reproduce Fe^{2+}, the reaction rate is much lower than that of the oxidation rate of Fe^{2+} to Fe^{3+} [18–23]. This further reduces the overall oxidation efficiency and requires continuous addition of Fe^{2+} salts [24], which results in a large amount of iron sludge to be disposed of [25]. This will result in an increase in the treatment cost of the Fenton reaction and potentially generate secondary pollution, which limits the application of homogeneous Fenton reactions in water treatment [25,26].

In recent years, many methods have been used to improve the treatment effect of the Fenton reaction. One strategy is to combine the Fenton reaction with other technologies, such as the introduction of light, electricity, microwave, ultrasound, and other technologies e named photo-Fenton, electro-Fenton, photo-electro-Fenton, microwave-driven Fenton, etc. [11,27–31]. This strategy can widen the pH range at the Fenton process and reduce the amount of iron sludge [11,32]. Another strategy is to develop heterogeneous Fenton oxidation technology, which is to load iron elements on electron-rich material, such as metal oxide [7], metal–organic frameworks (MOFs) [33,34], graphene [35], carbon nanotubes [25], activated carbon [36,37], fullerene [38], and carbon nitride (C_3N_4) [39]. The iron source is uniformly supported or immobilized on such materials as small aggregates or clusters to enhance the Fe^{3+}/Fe^{2+} cycle and Fenton reaction efficiency [30,40]. The third strategy is to employ various reducing agents in the traditional homogeneous Fenton system to promote the reduction of Fe^{3+} to Fe^{2+}. Most of the reducing agents such as hydroxylamine [41], quinone hydroquinone [42], organic acid [43], boron [44], and activated carbon [45] are also electron-rich materials that can provide electrons to promote the conversion of Fe^{3+} to Fe^{2+}. However, these methods also have drawbacks. It requires a cost-sensitive and complex equipment system for the Fenton reaction to be combined with other technologies [46]. Meanwhile, the heterogeneous Fenton reaction is only suitable for the treatment of low-concentration pollutants [47,48], even when the concentration of organic matter considered in the heterogeneous catalytic study is very high (C_0 = 500 mg/L of methylene blue) [47], which is far less than the maximum concentration of organic matter (COD > 100,000 mg/L) that can be treated by the homogeneous Fenton reaction [5]. Adding hydroxylamine or boron into the homogeneous phase will lead to secondary pollution, and the addition of quinone hydroquinone or organic acids will increase the COD value in the water [42,44,49–51]. Therefore, a non-toxic and stable material that can convert Fe^{3+} to Fe^{2+} in a homogeneous Fenton reaction and further improve the treatment effect of the Fenton reaction should be adopted. In this way, the problem of increasing Fe^{2+} dosage due to Fe^{2+} oxidation can be improved, and the cost and production of iron sludge can be reduced.

Activated carbon (AC) is one of the carbonaceous materials with a large specific surface area, which can provide adequate dispersion and isolation of the catalytic sites and favors the interfacial contact of the substrate with the activated centers [52]. Therefore, AC has been widely used in adsorption and catalysis. In the application of the Fenton reaction, the adsorption effect of activated carbon can assist the removal of pollutants. At the same time, AC can also act as an electron donor and/or an electron shuttle to promote the reduction of low-cost Cr(VI) and Fe(III) [14,53,54]. This provides a theoretical basis for AC to promote Fe^{3+}/Fe^{2+} cycling in homogeneous Fenton reactions. In the study of the assistance effect of activated carbon on the Fe^{3+}/H_2O_2 system, the adsorption and reduction properties of activated carbon and the effect of the comprehensive performance of activated carbon on the degradation of pollutants in the Fe^{3+}/H_2O_2 system will be ignored. In fact, it is meaningful to select the best activated carbon through the treatment effect and the ability to reduce Fe^{3+}, study the influence of different influencing factors on the treatment effect of Fe^{3+}/H_2O_2/AC system, obtain the conditions with the best treatment effect, and further study the promoting effect of the reducing power of AC on Fe^{3+}/H_2O_2 and the reduction mechanism.

In this study, coconut shell-activated carbon (CSPAC), wood-activated carbon (WPAC), and coal-activated carbon (CPAC) were introduced into the Fe^{3+}/H_2O_2 system to study the positive effect of ACs in Fenton and Fenton-like reactions. The best activated carbon CSPAC was selected, and the effects of CSPAC dosage, initial H_2O_2 concentration, initial Fe^{3+} concentration, and pH on ARG degradation were investigated. The positive roles of CSPAC in improving the efficiency of ARG degradation and reduction efficiency of Fe^{3+} to Fe^{2+} in Fe^{3+}/H_2O_2 reaction system were also studied to boost the application of Fenton or Fenton-like processes with ACs in the degradation of organic pollutions from wastewater.

2. Materials and Methods

2.1. Materials

Chemicals used in this study include ferric chloride hexahydrate ($FeCl_3 \cdot 6H_2O$), ferrous chloride tetrahydrate ($FeCl_2 \cdot 4H_2O$), hydrogen peroxide (H_2O_2), sodium hydroxide (NaOH), hydrochloric acid (HCl), potassium dichromate ($K_2Cr_2O_7$), silver sulfate (Ag_2SO_4), mercury sulfate ($HgSO_4$), glacial acetic acid, sodium acetate, hydroxylamine hydrochloride, potassium permanganate, and methanol and were purchased from Sinopharm Chemical Reagent Co., Ltd., activated carbon (AC) was from Suzhou Carbon Cyclone Activated Carbon Co., Ltd., Acid red G (ARG) was from Tianjin Fine Chemical Co., Ltd., Tianjin, China, and 1,10-Phenanthroline from Sahn Chemical Technology (Shanghai, China) Co., Ltd. All chemicals were of reagent grade and used as received except the AC. ACs were acid-washed to remove impurities on the surface and then immersed in hydrochloric acid solution (10% *v*/*v*) for 24 h, filtered, and washed several times with deionized water. The obtained solids were dried at 110 °C for 6 h [55]. Meanwhile, ACs were milled and sieved through different meshes to obtain activated carbon powder with particle sizes of 1000 µm, 500 µm, 250 µm, 100 µm, 75 µm, and 50 µm, respectively, for the experiment. All the solutions were prepared in ultrapure water.

2.2. Characterization

The specific surface areas (SSAs) of the ACs were determined on an SSA analyzer (SSA-4300, Beijing Builder Electronic Technology Co., Ltd., Beijing, China) using the nitrogen adsorption–desorption method at 77 K (Brunauer–Emmett–Teller method), and the pore volumes were calculated by the Barrett–Joyner–Halenda method offered by the equipment. Fourier transform infrared spectroscopy (FT-IR) was used to characterize the chemical groups in the samples, and the FT-IR spectra in this study were acquired on a Bruker Tensor 37 infrared spectrometer (Bruker TENSOR 37 FT-IR) in the region from 400 to 4000 cm^{-1} by the KBr pellet method. X-ray photoelectron spectroscopy (XPS, Thermo Scientific EscaLab 250Xi) with the emission source of Al Kα (1486.71 eV) was used to analyze the composition of the surface elements of the ACs and the valence state of the samples. The C 1s electron binding energy (284.8 eV) was used as the standard to correct all the binding energies (BEs) [56].

2.3. Experimental Procedures

All experiments were conducted in a 250 mL glass beaker. The reaction was initiated with the addition of desired dosages of 200 mL of 100 mg/L Acid Red G (ARG), 0.01 mol/L $FeCl_3$, AC, and 0.1 mol/L H_2O_2. The beaker was placed in a constant temperature water bath controlled at 25 ± 1 °C. At each time interval, a 2 mL sample was withdrawn using a 2.5 mL syringe and filtered immediately using the cellulose acetate membrane with a pore diameter of 0.45 µm, and quenched by the addition of methanol. The desired initial pH was adjusted with 0.1 mol/L NaOH and 0.1 mol/L HCl before the reaction.

2.4. Analytical Methods

The characteristic wavelength of UV absorption (UV2600A, Unico, Shanghai, China) at 506 nm was used to detect the concentration of ARG [56]. The concentration of H_2O_2 was determined by titanium salt spectrophotometry. Fe^{2+} and Fe^{3+} were determined by 1,10-

Phenanthroline spectrophotometry [55,57]. A chemical oxygen demand (COD) detector (Multi-direct, Lovibond) was employed to detect COD [58].

According to the test data, ARG removal rate (η_{COLOR}%) and COD removal rate (η_{COD}%) were analyzed, and the calculation by Formula (1) and (2) [3,58]:

$$\eta_{COLOR}\% = \frac{(A_0 - A_t)}{A_0} \times 100\% \quad (1)$$

$$\eta_{COD}\% = \frac{(COD_0 - COD_t)}{COD_0} \times 100\% \quad (2)$$

where A_0 and A_t are the absorbance of ARG at the initial moment and the time of t, respectively, and COD_0 (mg/L) and COD_t (mg/L) are COD concentration in water at the initial time and time t.

3. Results and Discussion

3.1. Promotion of Fenton-Like Reaction by Different Kinds of ACs

The degradation of ARG by the Fe^{3+}/H_2O_2 system, introducing commercially available coconut shell-activated carbon (CSPAC), wood-activated carbon (WPAC), and coal-activated carbon (CPAC) respectively, was investigated. Through characterization, it was observed that the three kinds of ACs have different pore size distributions, specific surface areas, pore volumes, and average pore size (Figure S1 and Table S1). It can be seen from Figure 1a that ARG in the Fe^{3+}/H_2O_2 system without AC was slowly degraded in the early stage of the reaction, only a decolorization rate of 30% was achieved in the first 10 min, and a decolorization rate of 63% was achieved within 60 min. Nevertheless, when AC was added, the degradation rate of ARG significantly increased in the early stage. Decolorization rates of 84%, 65%, and 57% could be achieved in Fe^{3+}/H_2O_2/CSPAC, Fe^{3+}/H_2O_2/WPAC, and Fe^{3+}/H_2O_2/CPAC systems within 10 min, respectively. The final decolorization rates of 90%, 73%, and 73% could be achieved in the three reaction systems, indicating that the addition of AC can improve the initial decolorization rate of the Fe^{3+}/H_2O_2 system and the final decolorization. At the same time, the removal rate of COD after the addition of AC was also observed and is shown in Figure 1b. The addition of AC also improved the COD removal efficiency in the system to varying degrees. The promoting effect of AC may be due to its adsorption effect, which can improve the removal effect of ARG, and it is worth noting that AC may also interact with Fe^{3+} to promote the formation of Fe^{2+} to increase the decolorization rate of ARG. To further illustrate this speculation, adsorption experiments were performed on the three kinds of ACs, as well as the determination of Fe^{2+} concentration in the Fe^{3+}/AC system (Figure 2). It can be seen from Figure 2a that all three kinds of ACs have the ability to adsorb ARG 61%, 21%, and 15% decolorization rates at first 10 min, and 74%, 25%, and 17% decolorization rates within 60 min were achieved in CSPAC, WPAC, and CPAC systems, respectively, by adsorption. It is shown in Figure 2b that the three kinds of ACs were also able to reduce Fe^{3+} to Fe^{2+}. At 5 min, the concentration of Fe^{2+} in the solution including CSPAC, WPAC, and CPAC were 0.05 mmol/L, 0.01 mmol/L, and 0.005 mmol/L, respectively, which indicates that AC can improve the treatment effect of ARG by using its adsorption and reduction properties. By comparison, the adsorption capacity, the ability to reduce Fe^{3+}, and the final degradation effect of CSPAC were the best, so CSPAC was chosen as the object of study in the subsequent experiments. To avoid the effect of leaching iron ions on the experimental results, the concentration of iron ions in the solution after the addition of AC treated and untreated by acid solution was studied (Figure S2). The results illustrate that the acid treatment is conducive to avoiding interference caused by iron ion dissolution from AC.

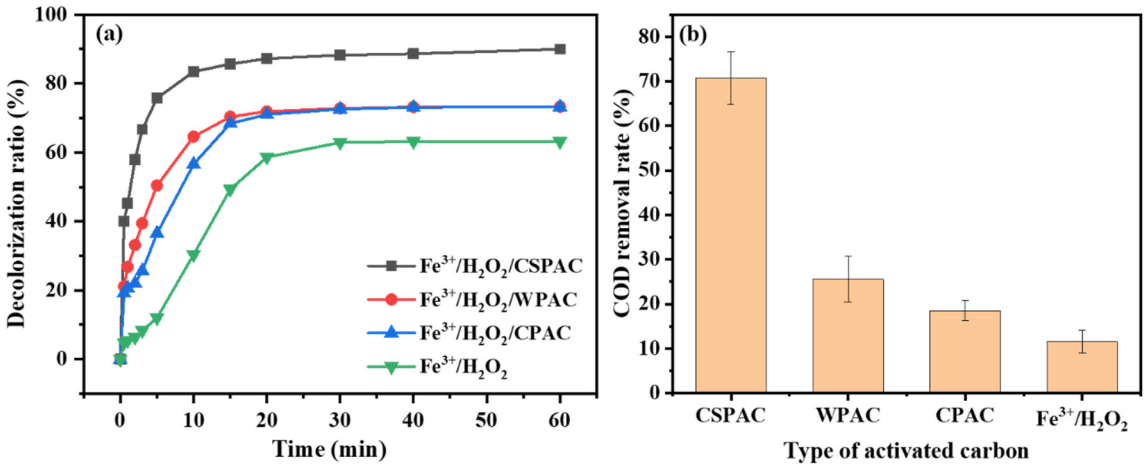

Figure 1. (**a**) Decolorization rate and (**b**) COD removal rate of ARG degradation in Fe^{3+}/H_2O_2/CSPAC, Fe^{3+}/H_2O_2/WPAC, Fe^{3+}/H_2O_2/CPAC, and Fe^{3+}/H_2O_2 systems (conditions: 0.1 mmol/L $FeCl_3$, 0.2 mmol/L H_2O_2, 100 mg/L ARG, 0.4 g/L PAC (75 μm particle size), pH = 3).

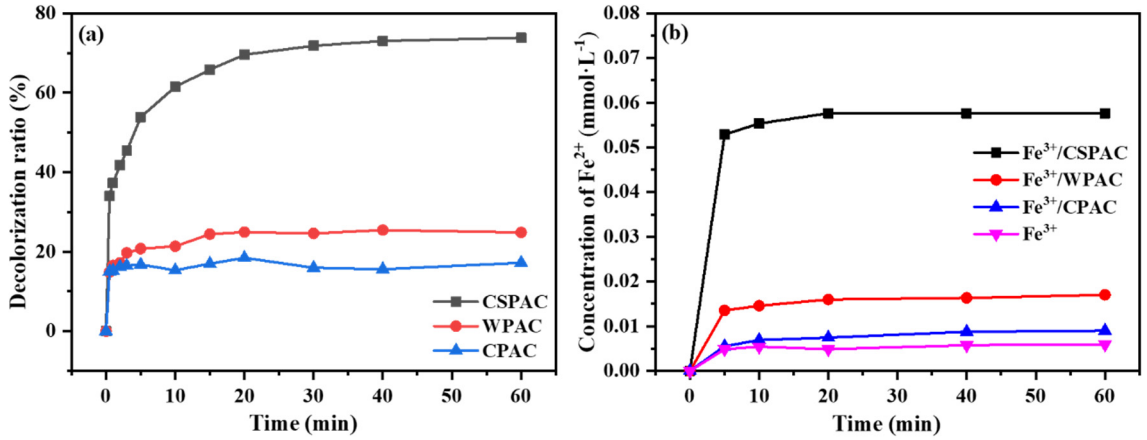

Figure 2. (**a**) Decolorization rate of ARG adsorption by CSPAC, WPAC, and CPAC (100 mg/L ARG, 0.4 g/L PAC (75 μm particle size), pH = 3). (**b**) Concentration of Fe^{2+} generation in Fe^{3+}/CSPAC, Fe^{3+}/WPAC, and Fe^{3+}/CPAC systems (0.1 mmol/L $FeCl_3$, 0.4 g/L PAC (75 μm particle size), pH = 3).

3.2. Influencing Factors of Fe^{3+}/H_2O_2/CSPAC System

The different particle sizes and concentrations of CSPAC affect the adsorption and reduction properties of CSPAC, which will have the effect of CSPAC in a Fenton-like reaction. As the oxidant and the source of hydroxyl radical in the reaction, the concentration of H_2O_2 will affect the efficiency of Fenton and Fenton-like reactions. The different concentrations of Fe^{3+} affect the decomposition rate of H_2O_2, so the concentration of Fe^{3+} is also a factor affecting the efficiency of Fenton and Fenton-like reactions. The value of pH is also an important factor in Fenton and Fenton-like reactions. So the effects of particle size and dosages of CSPAC, H_2O_2 concentration, Fe^{3+} concentration, and pH on the degradation of ARG were systematically investigated.

Figure 3 shows the decolorization of ARG, COD removal rate, and Fe^{3+} reduction performance in the Fe^{3+}/H_2O_2/CSPAC system under different CSPAC particle sizes. As can be seen in Figure 3a, the decolorization rate of ARG had been accelerated in the early stage than that of the Fe^{3+}/H_2O_2 system with the decrease in particle size, and the overall treatment efficiency was also improved. The COD removal rate also increased with the decrease in CSPAC particle size (Figure 3b). This is because the adsorption performance of CSPAC increases as the particle size decreases, while the reduction performance of Fe^{3+}

was also increased (Figure 3c). However, when the particle size of CSPAC was too small, the improvement of decolorization rate and COD removal were not obvious, and the ability to reduce ferric ions would be slightly reduced, which may be because the particle size is too small to float on water when stirring, and it is not easy to stir evenly and the reaction is not sufficient. At the same time, the small particle size of activated carbon is not conducive to the settlement after the reaction and will increase the operation cost. Therefore, 75 μm was selected as the best CSPAC particle size for the subsequent study.

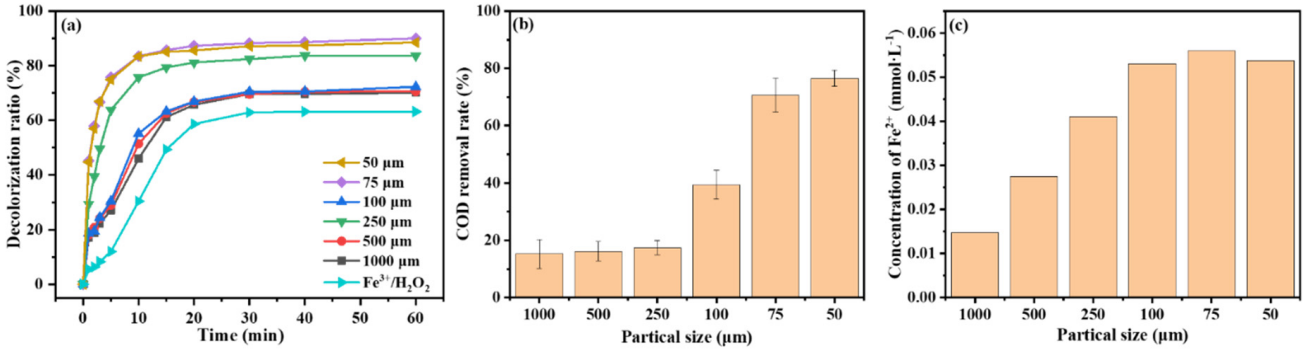

Figure 3. Effect of different CSPAC particle sizes on the (**a**) decolorization rate of ARG, (**b**) COD removal rate in the Fe^{3+}/H_2O_2/CSPAC system (0.1 mmol/L $FeCl_3$, 0.2 mmol/L H_2O_2, 100 mg/L ARG, 0.4 g/L CSPAC (50–1000 μm), pH = 3), and (**c**) generation of Fe^{2+} in the Fe^{3+}/CSPAC system (0.1 mmol/L $FeCl_3$, 0.4 g/L CSPAC (50–1000 μm), pH = 3).

The decolorization of ARG and COD removal rate in the Fe^{3+}/H_2O_2/CSPAC system at different CSPAC concentrations and the reduction of Fe^{3+} at different CSPAC concentrations are depicted in Figure 4. It can be seen that in the range of CSPAC concentration of 0–0.6 g/L, the adsorption of ARG and reduction of Fe^{3+} can be promoted by the increase in CSPAC concentration, which further enhanced both the decolorization rate and COD removal rate. When the CSPAC concentration exceeded 0.6 g/L and increased to 0.8 g/L, the COD removal rate decreased. Therefore, 0.6 g/L was chosen as the optimum concentration of CSPAC for the subsequent experiments.

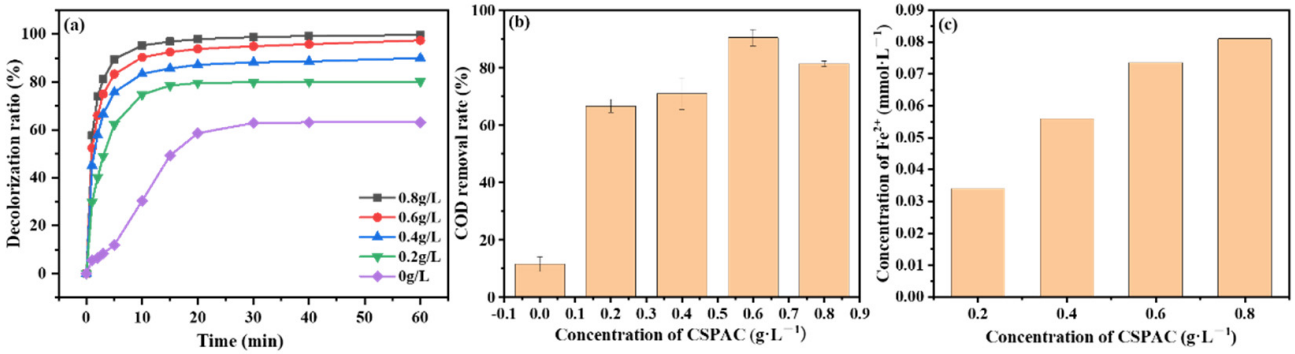

Figure 4. Effect of different CSPAC concentrations on the (**a**) decolorization rate of ARG, (**b**) COD removal rate in the Fe^{3+}/H_2O_2/CSPAC system (0.1 mmol/L $FeCl_3$, 0.2 mmol/L H_2O_2, 100 mg/L ARG, 0–0.8 g/L CSPAC (75 μm particle size), pH = 3), and (**c**) generation of Fe^{2+} in the Fe^{3+}/CSPAC system (0.1 mmol/L $FeCl_3$, 0–0.8 g/L CSPAC (75 μm particle size), pH = 3).

The ARG decolorization rate and the COD removal rate in the Fe^{3+}/H_2O_2/CSPAC system at different H_2O_2 concentrations are depicted in Figure 5. It can be seen that the COD removal rates at different H_2O_2 concentrations are all high, which is because the adsorption performance of CSPAC can improve COD removal and maintain COD removal even at very low H_2O_2 concentrations. However, too low of a H_2O_2 concentration would

reduce the decolorization rate of ARG. When the H_2O_2 concentration was over 0.4 mmol/L, the decolorization rate of ARG did not increase much when increasing H_2O_2 concentration. Therefore, 0.4 mmol/L was selected as the optimal H_2O_2 concentration for the subsequent experiments in terms of the ARG decolorization rate, COD removal rate and economy.

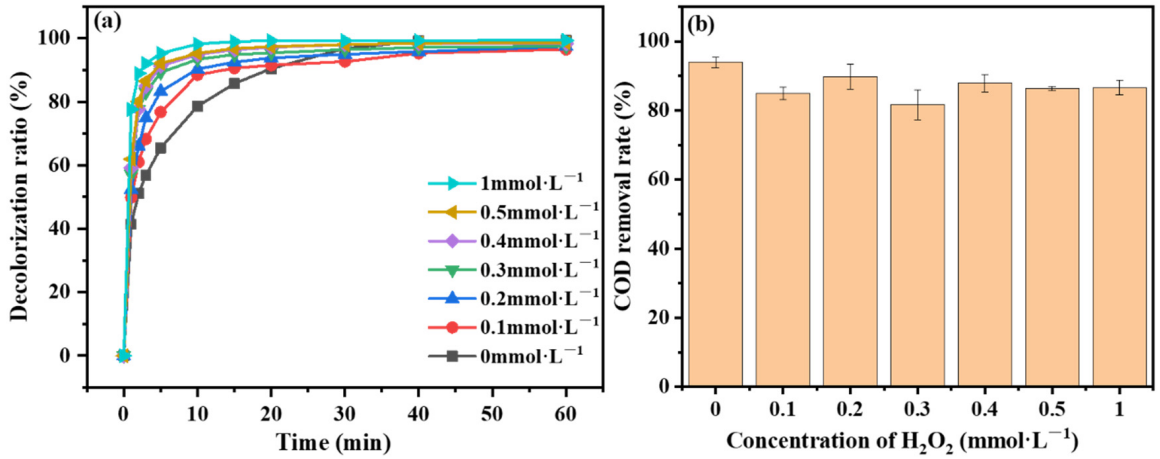

Figure 5. Effect of different H_2O_2 concentrations on the (**a**) decolorization rate of ARG and (**b**) COD removal rate in the Fe^{3+}/H_2O_2/CSPAC system (0.1 mmol/L $FeCl_3$, 0–1 mmol/L H_2O_2, 100 mg/L ARG, 0.6 g/L CSPAC (75 μm particle size), pH = 3).

The ARG decolorization rate and the COD removal rate in the Fe^{3+}/H_2O_2/CSPAC system at different Fe^{3+} concentrations are depicted in Figure 6. As can be seen in Figure 6, after the addition of Fe^{3+}, the decolorization rate is improved to a certain extent, but the COD removal rate is decreased, compared with the situation where the adsorption capacity of activated carbon is used to remove pollutants without Fe^{3+}, indicating that the addition of Fenton oxidation does not promote the degradation of COD. With the increase in Fe^{3+} concentration, the oxidation capacity was enhanced, and the decolorization rate and COD began to increase. When the concentration of Fe^{3+} rose to 0.1 mmol/L, the decolorization rate and COD removal rate did not change significantly with the increase in the concentration of Fe^{3+}, which may be due to the limitation of hydrogen peroxide. Considering the decolorization rate, COD removal rate, and economic benefits, 0.1 mmol/L was selected as the optimal Fe^{3+} concentration for subsequent experiments.

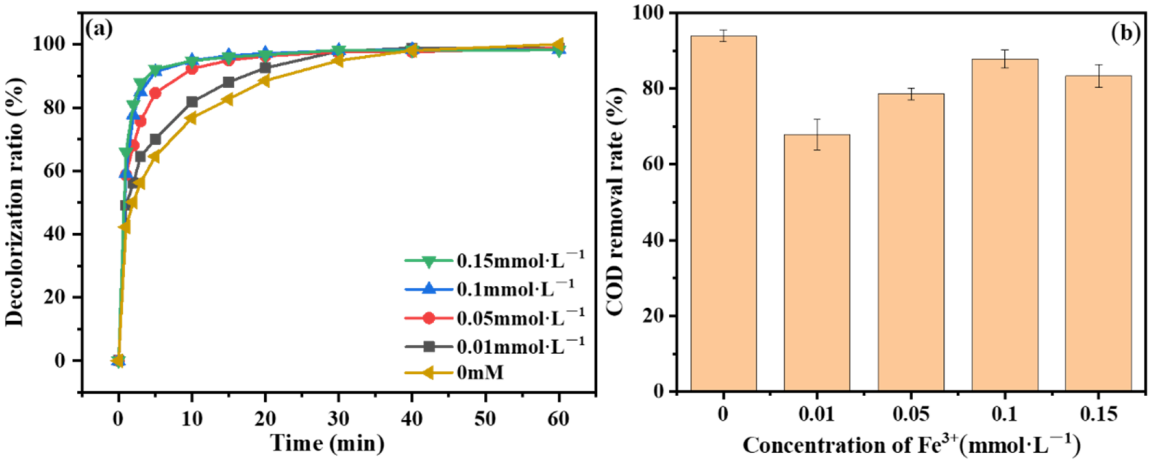

Figure 6. Effect of different Fe^{3+} concentrations on the (**a**) decolorization rate of ARG and (**b**) COD removal rate in the Fe^{3+}/H_2O_2/CSPAC system (0–0.15 mmol/L $FeCl_3$, 0.4 mmol/L H_2O_2, 100 mg/L ARG, 0.6 g/L CSPAC (75 μm particle size), pH = 3).

The ARG decolorization rate and the COD removal rate in the Fe^{3+}/H_2O_2/CSPAC system at different pH conditions are depicted in Figure 7. It can be seen that the decolorization rate and COD removal rate at pH 2.5 are smaller than those at pH 3, because with a lower pH, too much H+ in the solution destroyed the balance between Fe^{2+} and Fe^{3+}, affecting the generation of the hydroxyl radicals, thereby reducing the oxidation ability of Fenton reaction, and affecting the removal of pollutants by the Fe^{3+}/H_2O_2/CSPAC system [59,60]. When pH > 3, this promoted Fe^{2+} and Fe^{3+} to convert to hydrogenate precipitation. The oxidation properties of the Fenton reaction will be reduced [59,60], so the decolorization rate will decrease. However, the adsorption capacity of CSPAC is strong, and the COD removal rate remains very high. Because pH > 3 is not conducive to the subsequent study of the Fenton reaction in the system, pH = 3 is finally selected as the best condition for subsequent experiments.

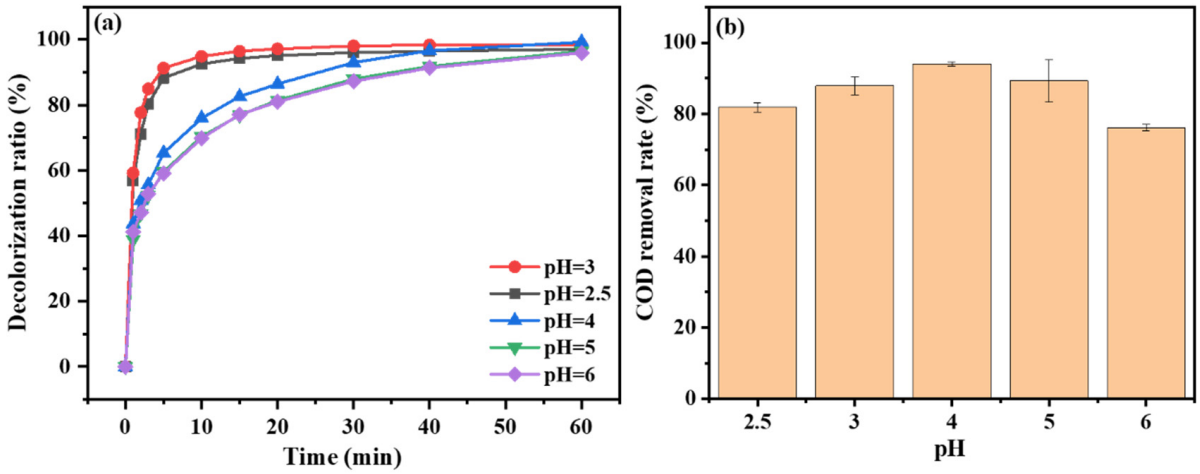

Figure 7. Effect of different pH on the (**a**) decolorization rate of ARG and (**b**) COD removal rate in the Fe^{3+}/H_2O_2/CSPAC system (0.1 mmol/L $FeCl_3$, 0.4 mmol/L H_2O_2, 100 mg/L ARG, 0.6 g/L CSPAC (75 μm particle size), pH = 2.5–6).

3.3. Performance of CSPAC Enhanced Fe^{3+}/H_2O_2 Oxidation

To further understand the oxidation performance enhancement of the Fe^{3+}/H_2O_2 system by the addition of CSPAC, the degradation of ARG in the single CSPAC system, Fe^{3+}/CSPAC, H_2O_2/CSPAC, Fe^{3+}/H_2O_2, and Fe^{3+}/H_2O_2/CSPAC systems were investigated, respectively. As shown in Figure 8a, only about 77% of the decolorization rate was achieved in the Fe^{3+}/H_2O_2 system, but the reaction rate was slow in the early stage. However, the decolorization rate of ARG in the single CSPAC system, Fe^{3+}/CSPAC system, and H_2O_2/CSPAC system could reach 99% after adding CSPAC, which is due to the strong adsorption ability of CSPAC. It can be seen from Figure 8a that the treatment effects of CSPAC, Fe^{3+}/CSPAC, and H_2O_2/CSPAC systems are the same, indicating that adding Fe^{3+} and H_2O_2 systems alone to CSPAC does not promote the removal of pollutants. Since the strong adsorption performance of CSPAC would mask other effects of CSPAC, the decolorization in Fe^{3+}/H_2O_2 and Fe^{3+}/H_2O_2/CSPAC systems was investigated after reducing the adsorption performance of CSPAC. As shown in Figure 8b, it can be seen that a decolorization rate of 61.8% was achieved at the first 5 min in the Fe^{3+}/H_2O_2/CSPAC system, which is much greater than that of the Fe^{3+}/H_2O_2 system (only 26.0%) and single CSPAC adsorption (only 21.7%), indicating that the addition of CSPAC exhibits a certain degree of acceleration in the Fe^{3+}/H_2O_2 system decolorization rate of ARG in the early reaction stage. Then the final decolorization effect is basically the same due to the limited hydrogen peroxide. Additionally, as can be seen in Figure 8, the CSPAC with reduced adsorption properties and untreated CSPAC were added to the Fe^{3+}/H_2O_2 system. Through the contrast of the decolorization curves, it can be seen that untreated CSPAC in the initial stages has a faster decolorization rate and a better decolorization effect. This indicates that

the adsorption property of CSPAC can promote the decolorization rate of ARG at the initial stage and can improve the decolorization effect of ARG in the Fe^{3+}/H_2O_2/CSPAC system.

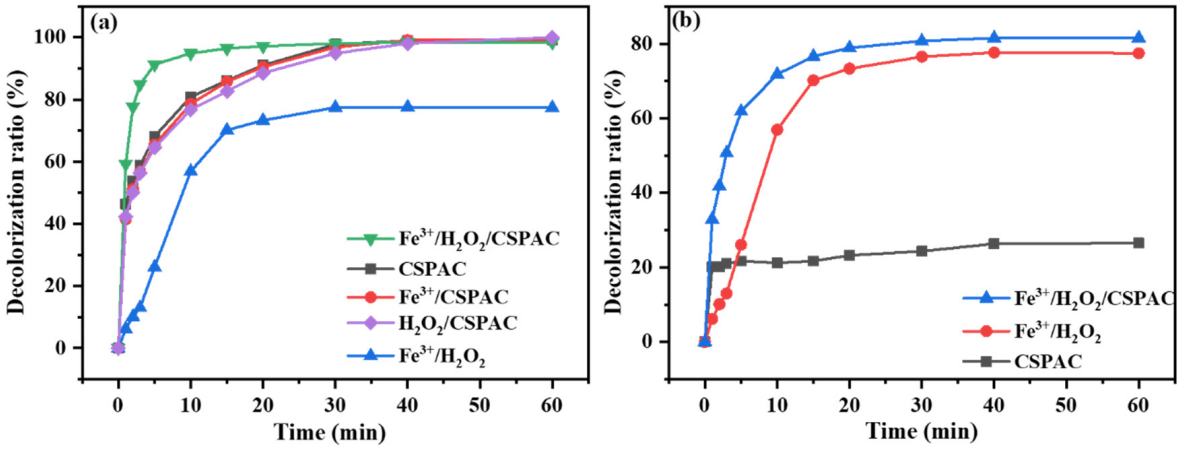

Figure 8. Decolorization rate of ARG in different systems under (**a**) untreated and (**b**) adsorbed saturated CSPAC conditions (0.1 mmol/L $FeCl_3$, 0.4 mmol/L H_2O_2, 100 mg/L ARG, 0.6 g/L CSPAC (75 μm particle size), pH = 3).

To further study the performance of CSPAC to accelerate the degradation of ARG in the Fe^{3+}/H_2O_2/CSPAC system, Fe^{2+} and H_2O_2 were monitored during the reaction. From Figure 9a, it can be seen that the final concentration of Fe^{2+} in the Fe^{3+}/H_2O_2 system was 0.007 mmol/L, and the final concentration of Fe^{2+} in the Fe^{3+}/CSPAC system increased to 0.076 mmol/L, up to 10 times higher, which illustrates the ability of CSPAC reduce Fe^{3+} to Fe^{2+}. After the addition of CSPAC to the Fe^{3+}/H_2O_2 system, the concentration of Fe^{2+} decreased rapidly compared with the Fe^{3+}/CSPAC system due to the rapid reaction between H_2O_2 and the generated Fe^{2+}. To verify this, the different systems were compared in terms of their ability to degrade H_2O_2. From Figure 9b, only about 8% of H_2O_2 was consumed in the Fe^{3+}/H_2O_2 system, and about 35% of H_2O_2 was degraded in the H_2O_2/CSPAC system, while the H_2O_2 consumption in the Fe^{3+}/H_2O_2/CSPAC system was significantly increased by more than 95%. It can also be observed that the concentration of Fe^{2+} started to increase after 20 min in the Fe^{3+}/H_2O_2/CSPAC system (Figure 9a) when the H_2O_2 concentration in the system almost reduced to zero (Figure 9b). These results indicate the positive role of activated carbon in Fenton and Fenton-like reactions.

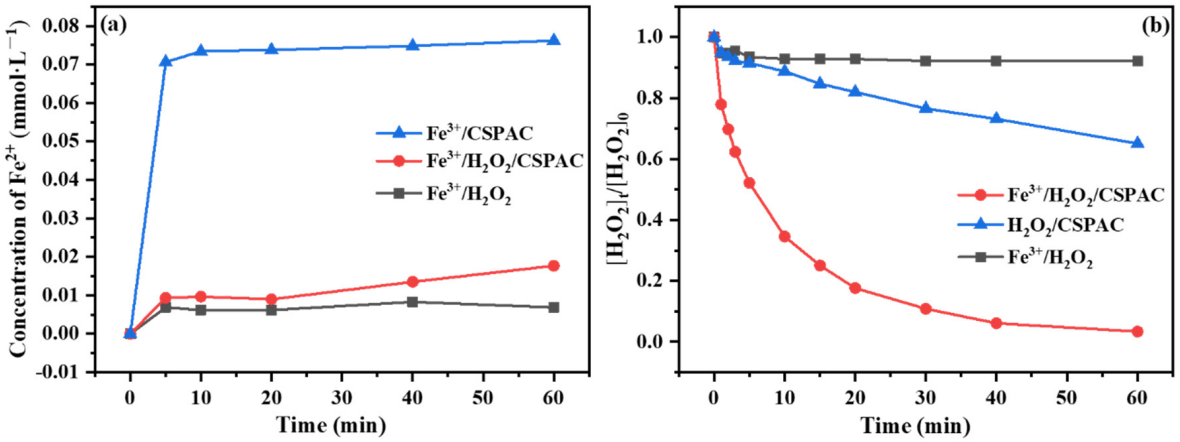

Figure 9. (**a**) Generation of Fe^{2+} and (**b**) degradation of H_2O_2 in different systems (0.1 mmol/L $FeCl_3$, 0.4 mmol/L H_2O_2, 0.6 g/L CSPAC (75 μm particle size), pH = 3).

3.4. The Catalytic Process of CSPAC during the Reaction

The changes of CSPAC surface groups before and after the reaction of different systems were observed by FT-IR and XPS to reveal the mechanism of the reduction of Fe^{3+} by CSPAC during the Fenton reaction. Figure 10 shows the FT-IR spectra of CSPAC before and after the reaction in the Fe^{3+}/H_2O_2/CSPAC system as well as after the reaction in the Fe^{3+}/CSPAC system. The peak appearing near 3400 cm^{-1} corresponds to the stretching band of the hydroxyl functional group O-H [61], the peak at 1737 cm^{-1} corresponds to COOH [62], the peak at 1600-1400 cm^{-1} corresponds to the C=C bond of the aromatic ring in AC structure [63], and the peak at 1088 cm^{-1} corresponds to the C-O stretching [63,64]. The CSPAC before the reaction contains O-H as well as C-O functional groups, while the peak at 1737 cm^{-1} is very weak and almost absent, while after the reaction, a more obvious peak at 1737 cm^{-1} appears, which indicates that CSPAC was oxidized and carboxyl groups are produced during the reaction. To further investigate the role of Fe^{3+} in the reaction process, the FT-IR spectrum of CSPAC after degradation of ARG in the Fe^{3+}/CSPAC system was also tested, and it can be seen that CSPAC also showed a more obvious peak at 1737 cm^{-1} after the reaction, which indicates that Fe^{3+} can oxidize a portion of organic groups on CSPAC surface during the reaction. So a portion of carbons on the surface of CSPAC was oxidized to form carboxyl groups by Fe^{3+} and thus Fe^{3+} was reduced to Fe^{2+} at the same time.

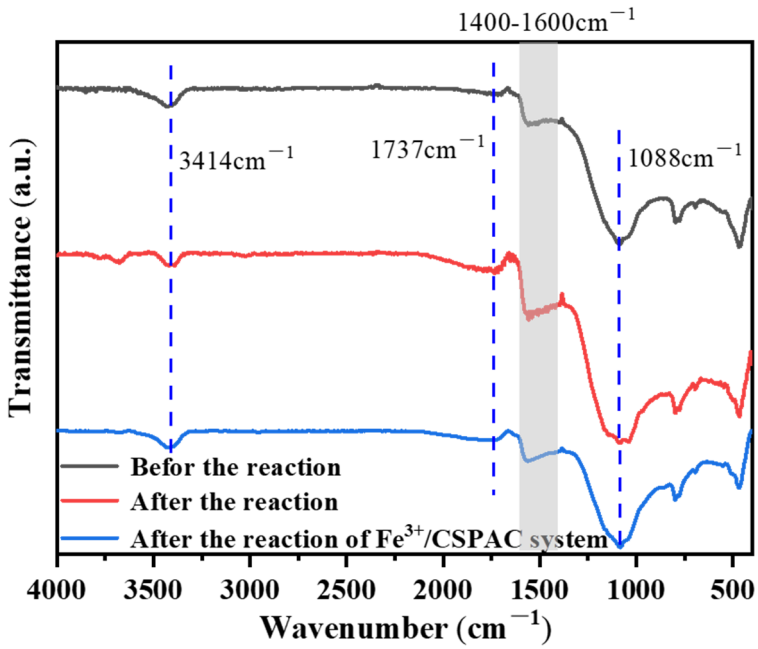

Figure 10. FT-IR spectra of CSPAC before and after the reaction in the Fe^{3+}/H_2O_2/CSPAC system, and after reaction in the Fe^{3+}/CSPAC system.

The chemical states of C and O elements in CSPAC were further analyzed using X-ray photoelectron spectroscopy. By comparing the full-scan spectra of CSPAC before and after the reaction (Figure S3), the percentage of O 1s increased from 15.8% to 17.4%, while the percentage of C 1s decreased from 84.2% to 82.6% due to the oxidation of the system, and the Fe species did not appear in CSPAC. Additionally, it can be seen from Figure S4 that CSPAC did not adsorb Fe^{3+} and Fe^{2+}, which indicated that CSPAC had almost no chelation with Fe^{3+} or Fe^{2+}. Figure 11 shows high-resolution C 1s spectra of CSPAC before and after the reaction, and after the reaction in the Fe^{3+}/CSPAC system. The values of 284.0 eV, 284.8 eV, 286 eV, and 288.9 eV, represent C=C, C-C, C-O, and C=O in the presence of carboxylate structure, respectively [65,66]. Figure 12 shows the high-resolution O 1s spectra of CSPAC before and after the reaction, and after the reaction in the Fe^{3+}/CSPAC system. The values of 532.3 eV, 533.5 eV, and 534.7 eV represent O-H in the hydroxyl

group, C-O, and C=O in the carboxyl group, respectively [65]. The results illustrate that the surface of CSPAC before the reaction contains C-O as well as O-H functional groups, which is consistent with the FT-IR characterization, and the presence of C=O in the carboxyl structure after the reaction indicates that CSPAC was oxidized after the reaction, which further indicates that CSPAC can reduce Fe^{3+} to Fe^{2+} while the reducing functional groups on the surface of CSPAC were oxidized to generate carboxyl groups.

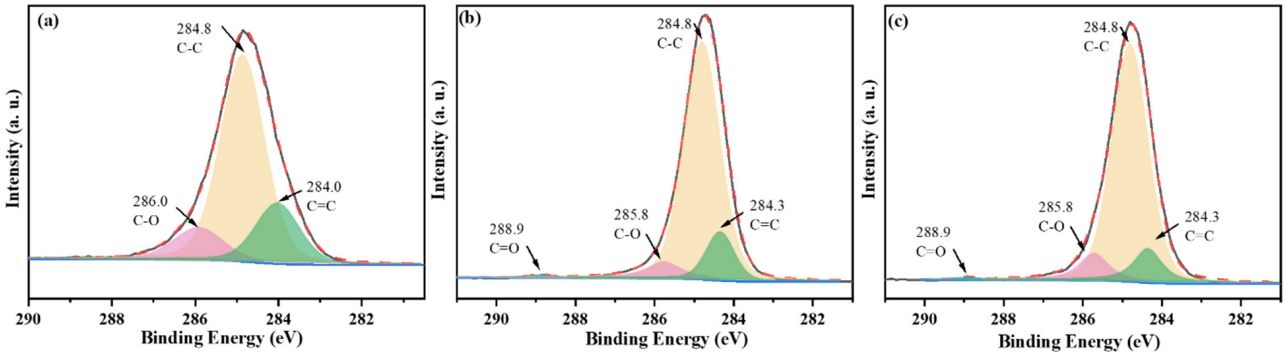

Figure 11. High-resolution C 1s spectra in CSPAC (**a**) before and (**b**) after the reaction in the Fe^{3+}/CSPAC/H_2O_2 system, and (**c**) after the reaction in the Fe^{3+}/CSPAC system.

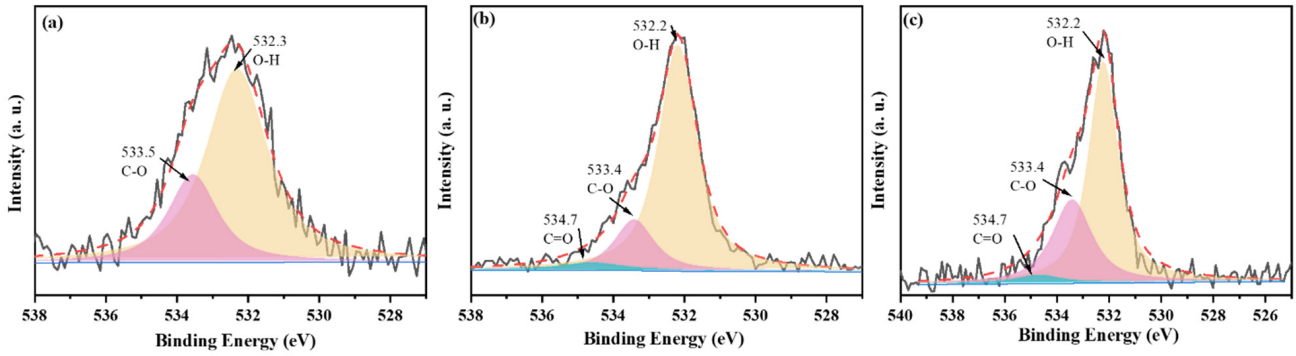

Figure 12. High-resolution O 1s spectra in CSPAC (**a**) before and (**b**) after the reaction in the Fe^{3+}/CSPAC/H_2O_2 system, and (**c**) after the reaction in the Fe^{3+}/CSPAC system.

Through the above characterization, it was observed that CSPAC has an O-H functional group, and it is speculated that the C-O-H group on the surface of CSPAC transfers electrons to Fe^{3+} and is oxidized to form the carboxyl group. To further prove that it was the C-O-H functional group on the surface of CSPAC that reduced Fe^{3+}, CSPAC was treated with 1 mol/L NaOH at 60 °C to increase the O-H on its surface. The reduction ability of CSPAC was compared with that of untreated CSPAC, and the results are shown in Figure 13. It can be seen from FT-IR spectra that, after NaOH treatment, the O-H content on CSPAC increased, which proved that O-H functional groups were successfully added on the surface of NaOH-CSPAC. Then, the Fe^{3+} reduction ability of the two CSPACs with or without NaOH treatment was compared, and the results are shown in Figure 13b. NaOH-CSPAC can generate 0.086 mmol/L of Fe^{2+}, which is higher than that of untreated CSPAC, 0.076mmol/L, indicating that the C-O-H group on the surface of CSPAC can reduce Fe^{3+} to Fe^{2+} and itself was oxidized into the carboxyl group.

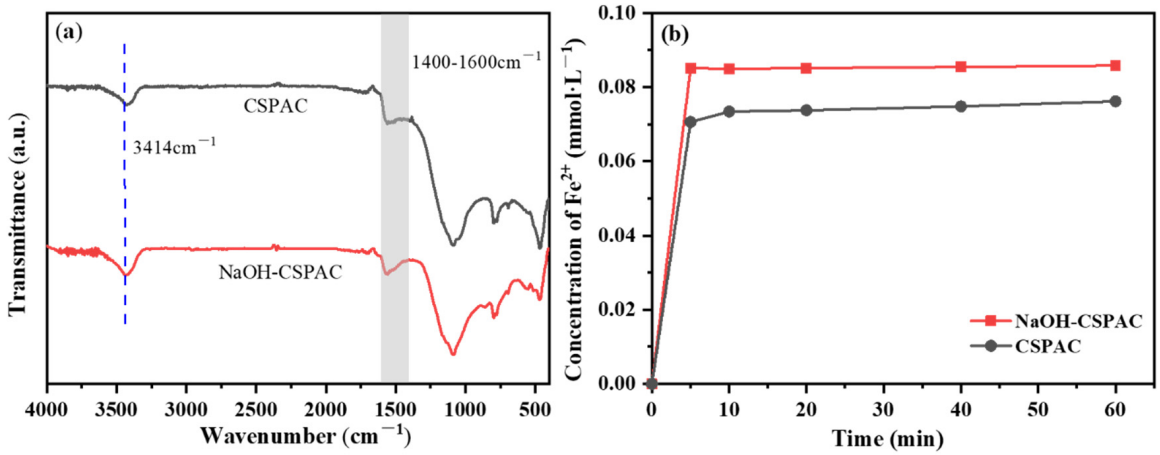

Figure 13. FT-IR spectra of NaOH-CSPAC and CSPAC (**a**) and concentrations of Fe^{2+} generated by NaOH-CSPAC and CSPAC in the Fe^{3+}/CSPAC system (**b**).

4. Conclusions

In this study, ACs were employed in the Fe^{3+}/H_2O_2 system, and the adsorption and reduction properties of ACs were used to significantly improve the removal of ARG in water. The results show that adding different types of ACs (coconut shell-activated carbon (CSPAC), wood-activated carbon (WPAC), and coal-activated carbon (CPAC)) to the Fe^{3+}/H_2O_2 system can improve the removal effect of ARG, and also confirm that AC has the ability to reduce Fe^{3+}, while different types of ACs have different treatment effects due to their different adsorption properties and ability to reduce Fe^{3+}. CSPAC exhibited the best performance in reducing Fe^{3+} to Fe^{2+} in the Fe^{3+}/H_2O_2 system. Different particle sizes and different concentrations of CSPAC, different concentrations of H_2O_2, different concentrations of Fe^{3+}, and different pH can affect the reaction efficiency of the Fe^{3+}/H_2O_2 system with CSPAC. CSPAC can reduce Fe^{3+} to Fe^{2+} and accelerate the consumption of H_2O_2, increasing the early stage of the reaction rate. The C-O-H on the surface of CSPAC is responsible for the reduction of Fe^{3+} to Fe^{2+} in water. This finding will provide useful information for understanding the chemistry of Fenton-like systems interacting with active carbon. In addition, the interaction between the adsorption and reduction properties of activated carbon in the Fe^{3+}/H_2O_2/CSPAC system, the interaction between the adsorption and oxidation in the Fe^{3+}/H_2O_2/CSPAC system, and the subsequent reuse of AC in iron mud are also worthy of further study.

Supplementary Materials: The following supporting information can be downloaded at: https://www.mdpi.com/article/10.3390/catal12111358/s1, Figure S1. N_2 adsorption–desorption isotherm of CSPAC (a), WPAC (c) and CPAC (e); pore diameter distribution of CSPAC (b), WPAC (d), and CPAC (f); Figure S2. Total iron ion concentration in solution (a) before and (b) after acid treatment; Figure S3. Full-scan XPS spectra of CSPAC before and after the reaction in Fe^{3+}/CSPAC/H_2O_2 system; Figure S4. Adsorption of (a) Fe^{3+} and (b) Fe^{2+} by CSPAC. Table S1. The specific surface area, pore size, and pore volume of three kinds of ACs.

Author Contributions: Conceptualization, J.F.; investigation, X.Y. and H.L.; writing—original draft preparation, X.Y. and J.F.; writing—review and editing, J.F., B.H., M.Z., and W.Y. All authors have read and agreed to the published version of the manuscript.

Funding: This research was funded by the National Natural Science Foundation of China (No. 52070155) and the Open Project of Jiangsu Engineering Laboratory of New Materials for Sewage Treatment and Recycling (No. SDGC2127).

Data Availability Statement: Not applicable.

Acknowledgments: Jiangtao Feng acknowledges the National Natural Science Foundation of China (No. 52070155) and the Open Project of Jiangsu Engineering Laboratory of New Materials for Sewage Treatment and Recycling (No. SDGC2127). Bo Hou acknowledges the support from Cardiff University, and the Royal Society of Chemistry (No. E21-9668828170). The authors also acknowledge the financial support from the IEC\NSFC\211201-International Exchanges 2021 Cost Share (NSFC) and the Instrumental Analysis Center of Xi'an Jiaotong University for the help in SEM, XPS testing, and analysis.

Conflicts of Interest: The authors declare no conflict of interest.

References

1. Bello, M.M.; Abdul Raman, A.A.; Asghar, A. A review on approaches for addressing the limitations of Fenton oxidation for recalcitrant wastewater treatment. *Process Saf. Environ. Prot.* **2019**, *126*, 119–140. [CrossRef]
2. Liu, Y.; Zhao, Y.; Wang, J.-L. Fenton/Fenton-like processes with in-situ production of hydrogen peroxide/hydroxyl radical for degradation of emerging contaminants: Advances and prospects. *J. Hazard. Mater.* **2021**, *404*, 124191. [CrossRef] [PubMed]
3. Yang, H.-H.; Shi, B.-F.; Wang, S.-L. Fe Oxides Loaded on Carbon Cloth by Hydrothermal Process as an Effective and Reusable Heterogenous Fenton Catalyst. *Catalysts* **2018**, *8*, 207. [CrossRef]
4. Partido, E.; Dominguez, J.R.; Torregrosa, J.; de Heredia, J.B. Degradation of wine distillery wastewaters by the combination of aerobic biological treatment with chemical oxidation by Fenton's reagent. *Water Sci. Technol.* **2005**, *51*, 167–174.
5. Hakika, D.C.; Sarto, S.; Mindaryani, A.; Hidayat, M. Decreasing COD in Sugarcane Vinasse Using the Fenton Reaction: The Effect of Processing Parameters. *Catalysts* **2019**, *9*, 881. [CrossRef]
6. Tang, J.-T.; Wang, J.-L. Fenton-like degradation of sulfamethoxazole using Fe-based magnetic nanoparticles embedded into mesoporous carbon hybrid as an efficient catalyst. *Chem. Eng. J.* **2018**, *351*, 1085–1094. [CrossRef]
7. Liu, X.-Y.; Zhang, Q.; Yu, B.-W.; Wu, R.-H.; Mai, J.-X.; Wang, R.-J.; Chen, L.-Y.; Yang, S.-T. Preparation of Fe3O4/TiO2/C Nanocomposites and Their Application in Fenton-Like Catalysis for Dye Decoloration. *Catalysts* **2016**, *6*, 146. [CrossRef]
8. Liu, X.-H.; Xie, L.-B.; Liu, Y.-G.; Zhao, P.; Han, Y.-G.; Cheng, S.-S.; Bai, X.-Y.; Li, Y. Rapid preparation of highly stable ZnO-CeO_2/CF cathode by one-step electro-deposition for efficient degradation of ciprofloxacin in electro-Fenton system. *Catal. Today* **2020**, *355*, 458–465. [CrossRef]
9. Wang, J.; Zhou, X.; Gatheru Waigi, M.; Owino Gudda, F.; Cheng, P.; Ling, W. Simultaneous Removal of Estrogens and Antibiotics from Livestock Manure Using Fenton Oxidation Technique. *Catalysts* **2019**, *9*, 644. [CrossRef]
10. Liu, X.-C.; Zhou, Y.-Y.; Zhang, J.-C.; Luo, L.; Yang, Y.; Huang, H.-L.; Peng, H.; Tang, L.; Mu, Y. Insight into electro-Fenton and photo-Fenton for the degradation of antibiotics: Mechanism study and research gaps. *Chem. Eng. J.* **2018**, *347*, 379–397. [CrossRef]
11. Gharaee, A.; Khosravi-Nikou, M.R.; Anvaripour, B. Hydrocarbon contaminated soil remediation: A comparison between Fenton, sono-Fenton, photo-Fenton and sono-photo-Fenton processes. *J. Ind. Eng. Chem.* **2019**, *79*, 181–193. [CrossRef]
12. Yu, G.-H.; Kuzyakov, Y. Fenton chemistry and reactive oxygen species in soil: Abiotic mechanisms of biotic processes, controls and consequences for carbon and nutrient cycling. *Earth Sci. Rev.* **2021**, *214*, 103525. [CrossRef]
13. Checa-Fernandez, A.; Santos, A.; Romero, A.; Dominguez, C.M. Application of Chelating Agents to Enhance Fenton Process in Soil Remediation: A Review. *Catalysts* **2021**, *11*, 722. [CrossRef]
14. Tang, Z.-M.; Zhao, P.-R.; Wang, H.; Liu, Y.-Y.; Bu, W.-B. Biomedicine Meets Fenton Chemistry. *Chem. Rev.* **2021**, *121*, 1981–2019. [CrossRef]
15. Wei, S.-B.; Qiao, Y.-Q.; Wu, Z.-C.; Liu, X.-M.; Li, Y.; Cui, Z.-D.; Li, C.-Y.; Zheng, Y.-F.; Liang, Y.-Q.; Li, Z.-Y.; et al. Na+ inserted metal-organic framework for rapid therapy of bacteria-infected osteomyelitis through microwave strengthened Fenton reaction and thermal effects. *Nano Today* **2021**, *37*, 101090. [CrossRef]
16. Neyens, E.; Baeyens, J. A review of classic Fenton's peroxidation as an advanced oxidation technique. *J. Hazard. Mater.* **2003**, *98*, 33–50. [CrossRef]
17. Zhang, M.-H.; Dong, H.; Zhao, L.; Wang, D.-X.; Meng, D. A review on Fenton process for organic wastewater treatment based on optimization perspective. *Sci. Total Environ.* **2019**, *670*, 110–121. [CrossRef]
18. Pignatello, J.J.; Oliveros, E.; MacKay, A. Advanced Oxidation Processes for Organic Contaminant Destruction Based on the Fenton Reaction and Related Chemistry. *Crit. Rev. Environ. Sci. Technol.* **2006**, *36*, 1–84. [CrossRef]
19. Lee, C.; Sedlak, D.L. A Novel Homogeneous Fenton-like System with Fe(III)-Phosphotungstate for Oxidation of Organic Compounds at Neutral pH Values. *J. Mol. Catal. A Chem.* **2009**, *311*, 1–6. [CrossRef]
20. Xu, T.-Y.; Zhu, R.-L.; Zhu, G.-Q.; Zhu, J.-X.; Liang, X.-L.; Zhu, Y.-P.; He, H.-P. Mechanisms for the enhanced photo-Fenton activity of ferrihydrite modified with BiVO 4 at neutral pH. *Appl. Catal. B.* **2017**, *212*, 50–58. [CrossRef]
21. Kwan, W.P.; Voelker, B.M. Decomposition of hydrogen peroxide and organic compounds in the presence of dissolved iron and ferrihydrite. *Environ. Sci. Technol.* **2002**, *36*, 1467–1476. [CrossRef] [PubMed]
22. Zhu, Y.-P.; Zhu, R.-L.; Xi, Y.-F.; Zhu, J.-X.; Zhu, G.-Q.; He, H.-P. Strategies for enhancing the heterogeneous Fenton catalytic reactivity: A review. *Appl. Catal. B.* **2019**, *255*, 117739. [CrossRef]
23. Hartmann, M.; Kullmann, S.; Keller, H. Wastewater treatment with heterogeneous Fenton-type catalysts based on porous materials. *J. Mater. Chem.* **2010**, *20*, 9002–9017. [CrossRef]

24. Bokare, A.D.; Choi, W. Review of iron-free Fenton-like systems for activating H_2O_2 in advanced oxidation processes. *J. Hazard. Mater.* **2014**, *275*, 121–135. [CrossRef] [PubMed]
25. Yang, Z.-C.; Yu, A.-Q.; Shan, C.; Gao, G.-D.; Pan, B.-C. Enhanced Fe(III)-mediated Fenton oxidation of atrazine in the presence of functionalized multi-walled carbon nanotubes. *Water Res.* **2018**, *137*, 37–46. [CrossRef] [PubMed]
26. Bolobajev, J.; Kattel, E.; Viisimaa, M.; Goi, A.; Trapido, M.; Tenno, T.; Dulova, N. Reuse of ferric sludge as an iron source for the Fenton-based process in wastewater treatment. *Chem. Eng. J.* **2014**, *255*, 8–13. [CrossRef]
27. Ganiyu, S.O.; Zhou, M.; Martínez-Huitle, C.A. Heterogeneous electro-Fenton and photoelectro-Fenton processes: A critical review of fundamental principles and application for water/wastewater treatment. *Appl. Catal. B.* **2018**, *235*, 103–129. [CrossRef]
28. Clarizia, L.; Russo, D.; Di Somma, I.; Marotta, R.; Andreozzi, R. Homogeneous photo-Fenton processes at near neutral pH: A review. *Appl. Catal. B.* **2017**, *209*, 358–371. [CrossRef]
29. Thor, S.-H.; Ho, L.-N.; Ong, S.-A.; Abidin, C.Z.A.; Heah, C.-Y.; Ong, Y.-P.; Yap, K.-L. A sustainable photocatalytic fuel cell integrated photo-electro-Fenton hybrid system using KOH activated carbon felt cathodes for enhanced Amaranth degradation and electricity generation. *Sep. Purif. Technol.* **2022**, *292*, 121041. [CrossRef]
30. Wang, Y.; Wang, R.-T.; Lin, N.-P.; Xu, J.-C.; Liu, X.-C.; Liu, N.; Zhang, X. Degradation of norfloxacin by MOF-derived lamellar carbon nanocomposites based on microwave-driven Fenton reaction: Improved Fe(III)/Fe(II) cycle. *Chemosphere* **2022**, *293*, 133614. [CrossRef]
31. Monteil, H.; Péchaud, Y.; Oturan, N.; Oturan, M.A. A review on efficiency and cost effectiveness of electro- and bio-electro-Fenton processes: Application to the treatment of pharmaceutical pollutants in water. *Chem. Eng. J.* **2019**, *376*, 119577. [CrossRef]
32. Brillas, E.; Garcia-Segura, S. Benchmarking recent advances and innovative technology approaches of Fenton, photo-Fenton, electro-Fenton, and related processes: A review on the relevance of phenol as model molecule. *Sep. Purif. Technol.* **2020**, *237*, 116337. [CrossRef]
33. Yang, T.-Y.; Yu, D.-Y.; Wang, D.; Yang, T.; Li, Z.-X.; Wu, M.-H.; Petru, M.; Crittenden, J. Accelerating Fe(III)/Fe(II) cycle via Fe(II) substitution for enhancing Fenton-like performance of Fe-MOFs. *Appl. Catal. B.* **2021**, *286*, 119859. [CrossRef]
34. Cheng, M.; Lai, C.; Liu, Y.; Zeng, G.-M.; Huang, D.-L.; Zhang, C.; Qin, L.; Hu, L.; Zhou, C.-Y.; Xiong, W.-P. Metal-organic frameworks for highly efficient heterogeneous Fenton-like catalysis. *Coord. Chem. Rev.* **2018**, *368*, 80–92. [CrossRef]
35. Su, S.-S.; Liu, Y.-Y.; Liu, X.-M.; Jin, W.; Zhao, Y.-P. Transformation pathway and degradation mechanism of methylene blue through beta-FeOOH@GO catalyzed photo-Fenton-like system. *Chemosphere* **2019**, *218*, 83–92. [CrossRef]
36. Wang, T.; Yang, C.C.; Qin, K.; Chen, C.W.; Dong, C.D. Life time enhanced Fenton-like catalyst by dispersing iron oxides in activated carbon: Preparation and reactivation through carbothermal reaction. *J. Hazard. Mater.* **2021**, *406*, 124791. [CrossRef]
37. Wang, C.-Q.; Sun, R.-R.; Huang, R. Highly dispersed iron-doped biochar derived from sawdust for Fenton-like degradation of toxic dyes. *J. Clean. Prod.* **2021**, *297*, 126681. [CrossRef]
38. Zou, C.-Y.; Meng, Z.-D.; Ji, W.-C.; Liu, S.-Q.; Shen, Z.; Zhang, Y.; Jiang, N.-S. Preparation of a fullerene [60]-iron oxide complex for the photo-fenton degradation of organic contaminants under visible-light irradiation. *Chin. J. Catal.* **2018**, *39*, 1051–1059. [CrossRef]
39. Lin, J.-K.; Tian, W.-J.; Guan, Z.-Y.; Zhang, H.-Y.; Duan, X.-G.; Wang, H.; Sun, H.-Q.; Fang, Y.-F.; Huang, Y.-P.; Wang, S.-B. Functional Carbon Nitride Materials in Photo-Fenton-Like Catalysis for Environmental Remediation. *Adv. Funct. Mater.* **2022**, *32*, 2201743. [CrossRef]
40. Peng, L.-J.; Duan, X.-G.; Shang, Y.-N.; Gao, B.-Y.; Xu, X. Engineered carbon supported single iron atom sites and iron clusters from Fe-rich Enteromorpha for Fenton-like reactions via nonradical pathways. *Appl. Catal. B.* **2021**, *287*, 119963. [CrossRef]
41. Wang, C.; Yu, G.-C.; Chen, H.; Wang, J.-L. Degradation of norfloxacin by hydroxylamine enhanced fenton system: Kinetics, mechanism and degradation pathway. *Chemosphere* **2020**, *270*, 129408. [CrossRef] [PubMed]
42. Duesterberg, C.K.; Waite, T.D. Kinetic modeling of the oxidation of p-hydroxybenzoic acid by Fenton's reagent: Implications of the role of quinones in the redox cycling of iron. *Environ. Sci. Technol.* **2007**, *41*, 4103–4110. [CrossRef] [PubMed]
43. Qin, Y.-X.; Song, F.-H.; Ai, Z.-H.; Zhang, P.-P.; Zhang, L.-Z. Protocatechuic Acid Promoted Alachlor Degradation in Fe(III)/H2O2 Fenton System. *Environ. Sci. Technol.* **2015**, *49*, 7948–7956. [CrossRef]
44. Zhou, P.; Ren, W.; Nie, G.; Li, X.-J.; Duan, X.-G.; Zhang, Y.-L.; Wang, S.-B. Fast and Long-Lasting Iron(III) Reduction by Boron Toward Green and Accelerated Fenton Chemistry. *Angew. Chem. Int. Ed. Engl.* **2020**, *59*, 16517–16526. [CrossRef] [PubMed]
45. Fontecha-Cámara, M.A.; Álvarez-Merino, M.A.; Carrasco-Marín, F.; López-Ramón, M.V.; Moreno-Castilla, C. Heterogeneous and homogeneous Fenton processes using activated carbon for the removal of the herbicide amitrole from water. *Appl. Catal. B.* **2011**, *101*, 425–430. [CrossRef]
46. Dogan, E.C.; Kilicoglu, O.; Narci, A.O.; Mert, B.K.; Durna, E.; Akbacak, U.A.; Aydiner, C. Fenton and photo-Fenton processes integrated with submerged ultrafiltration for the treatment of pulp and paper industry wastewater. *J. Environ. Chem. Eng.* **2021**, *9*, 105878. [CrossRef]
47. Lv, H.-L.; Zhao, H.-Y.; Cao, T.-C.; Qian, L.; Wang, Y.-B.; Zhao, G. Efficient degradation of high concentration azo-dye wastewater by heterogeneous Fenton process with iron-based metal-organic framework. *J. Mol. Catal. A Chem.* **2015**, *400*, 81–89. [CrossRef]
48. Tian, Y.-S.; Fu, W.-Y.; Wang, Q.; Tang, Y.-P.; Zhou, M. High electron transfer rate and efficiency on Fe0 modified by sulfidation and pre-magnetization for carbamazepine degradation by heterogeneous electro-Fenton in wide pH ranges. *Chem. Eng. J.* **2022**, *427*, 131694. [CrossRef]

49. Chen, L.-W.; Ma, J.; Li, X.-C.; Zhang, J.; Fang, J.-Y.; Guan, Y.-H.; Xie, P.-C. Strong Enhancement on Fenton Oxidation by Addition of Hydroxylamine to Accelerate the Ferric and Ferrous Iron Cycles. *Environ. Sci. Technol.* **2011**, *45*, 3925–3930. [CrossRef]
50. Li, T.; Zhao, Z.-W.; Wang, Q.; Xie, P.-F.; Ma, J.-H. Strongly enhanced Fenton degradation of organic pollutants by cysteine: An aliphatic amino acid accelerator outweighs hydroquinone analogues. *Water Res.* **2016**, *105*, 479–486. [CrossRef]
51. Ren, H.-J.; Jin, X.; Li, C.-G.; Li, T.-T.; Liu, Y.; Zhou, R. Rosmarinic acid enhanced Fe(III)-mediated Fenton oxidation removal of organic pollutants at near neutral pH. *Sci. Total Environ.* **2020**, *736*, 139528. [CrossRef] [PubMed]
52. Navalon, S.; Dhakshinamoorthy, A.; Alvaro, M.; Garcia, H. Heterogeneous fenton catalysts based on activated carbon and related materials. *ChemSusChem* **2011**, *4*, 1712–1730. [CrossRef] [PubMed]
53. Wang, H.-Z.; Guo, W.-Q.; Yin, R.-L.; Du, J.-S.; Wu, Q.-L.; Luo, H.-C.; Liu, B.-H.; Sseguya, F.; Ren, N. Biochar-induced Fe(III) reduction for persulfate activation in sulfamethoxazole degradation: Insight into the electron transfer, radical oxidation and degradation pathways. *Chem. Eng. J.* **2019**, *362*, 561–569. [CrossRef]
54. Zhou, L.; Liu, Y.-G.; Liu, S.-B.; Yin, Y.-C.; Zeng, G.-M.; Tan, X.-F.; Hu, X.; Hu, X.-J.; Jiang, L.-H.; Ding, Y.; et al. Investigation of the adsorption-reduction mechanisms of hexavalent chromium by ramie biochars of different pyrolytic temperatures. *Bioresour. Technol.* **2016**, *218*, 351–359. [CrossRef]
55. Seo, J.; Lee, H.-J.; Lee, H.; Kim, H.-E.; Lee, J.-Y.; Kim, H.S.; Lee, C. Enhanced production of reactive oxidants by Fenton-like reactions in the presence of carbon materials. *Chem. Eng. J.* **2015**, *273*, 502–508. [CrossRef]
56. Shi, B.-F.; Zhao, C.-C.; Ji, Y.-J.; Shi, J.-W.; Yang, H.-H. Promotion effect of PANI on Fe-PANI/Zeolite as an active and recyclable Fenton-like catalyst under near-neutral condition. *Appl. Surf. Sci.* **2020**, *508*, 145298. [CrossRef]
57. Harvey, A.E.; Smart, J.A.; Amis, E.S. Simultaneous Spectrophotometric Determination of Iron(II) and Total Iron with 1,10-Phenanthroline. *Anal. Chem.* **2002**, *27*, 26–29. [CrossRef]
58. Qiao, D.; Xu, Z.-C.; Guo, H.; Wang, X.; Wan, D.; Li, X.-Y.; Xu, H.; Yan, W. Non-traditional power supply mode: Investigation of electrodeposition towards a better understanding of PbO2 electrode for electrochemical wastewater treatment. *Mater. Chem. Phys.* **2022**, *284*, 126066. [CrossRef]
59. Bello, M.M.; Raman, A.A.A.; Asghar, A. Activated carbon as carrier in fluidized bed reactor for Fenton oxidation of recalcitrant dye: Oxidation-adsorption synergy and surface interaction. *J. Water Process Eng.* **2020**, *33*, 101001. [CrossRef]
60. Shen, L.; Wang, W.; Li, T.; Cui, Y.-Z.; Wang, B.; Yu, G.; Wang, X.-H.; Wei, D.; Xiao, J.-Z.; Deng, S.-B. Powdered activated coke for COD removal in the advanced treatment of mixed chemical wastewaters and regeneration by Fenton oxidation. *Chem. Eng. J.* **2019**, *371*, 631–638. [CrossRef]
61. Mendez, A.; Tarquis, A.M.; Saa-Requejo, A.; Guerrero, F.; Gasco, G. Influence of pyrolysis temperature on composted sewage sludge biochar priming effect in a loamy soil. *Chemosphere* **2013**, *93*, 668–676. [CrossRef] [PubMed]
62. Liu, X.-L.; Yin, H.-L.; Lin, A.-L.; Guo, Z.-Q. Effective removal of phenol by using activated carbon supported iron prepared under microwave irradiation as a reusable heterogeneous Fenton-like catalyst. *J. Environ. Chem. Eng.* **2017**, *5*, 870–876. [CrossRef]
63. Shin, S.; Jang, J.; Yoon, S.H.; Mochida, I. A study on the effect of heat treatment on functional groups of pitch based activated carbon fiber using FTIR. *Carbon* **1997**, *35*, 1739–1743. [CrossRef]
64. Zhao, W.-K.; Zhou, B. Assessing the role of CNTs in H2O2/Fe(III) Fenton-like process: Mechanism, DFT calculations and ecotoxicity evaluation. *Sep. Purif. Technol.* **2021**, *259*, 118218. [CrossRef]
65. Li, N.; Zhu, J.; Zha, Q.-F. Quantitative and qualitative analyses of oxygen-containing surface function groups on activated carbon. *Chem. J. Chin. Univ.* **2012**, *33*, 548–554.
66. Zhang, Z.-J.; Cui, P.; Chen, X.-Y.; Liu, J.-W. The production of activated carbon from cation exchange resin for high-performance supercapacitor. *J. Solid. State Electr.* **2013**, *17*, 1749–1758. [CrossRef]